PAPER

Check for updates

Comparative study on radiation resistance of tin–lead and pure lead perovskite solar cells

Longlong Zhang, [ID] [a] Shiqi Li,*[b] Yinghao Wang,[a] Hongwei Li,[a] Rui Chen,*[a] Xiang Zhu,[a] Xiaoheng Xu,[a] Yuying Hao [ID] [b] and Yingqi Ma*[a]

Perovskite solar cells (PSCs) offer promising opportunities for reducing the cost of space power. However, their radiation tolerance in the harsh space environment remains a critical requirement. In this work, we demonstrate that tin–lead (Sn–Pb) mixed perovskite, which enables the fabrication of all-perovskite tandem solar cells, exhibits significantly enhanced radiation resistance compared to conventional lead-only perovskites. A total ionizing dose (TID) test reveals that the power conversion efficiency (PCE) of $CH_3NH_3Pb_{0.7}Sn_{0.3}I_3$ PSCs decreases by 31% after exposure to 0.75 kGy and by 67% after 10 kGy γ-ray irradiation. In contrast, $CH_3NH_3PbI_3$ based devices suffer from much greater degradation, with PCE reductions of 48% and 90%, respectively. Considering the origins of such difference in radiation-induced PCE gradation, we find that the $CH_3NH_3Pb_{0.7}Sn_{0.3}I_3$ film retains its crystalline structure even after 10 kGy radiation, whereas $CH_3NH_3PbI_3$ is completely degraded. Based on Monte-Carlo simulations, we find that the formation of the critical radiation-induced defects, iodine vacancies and interstitial iodine, which are known as the primary defects to disrupt the perovskite lattice, is significantly suppressed in Sn–Pb mixed perovskites. Furthermore, we find that while interstitial iodines act as deep-level defects in $CH_3NH_3PbI_3$, they behave as shallow-level defects in $CH_3NH_3Pb_{0.7}Sn_{0.3}I_3$. This difference further reduces the impact of radiation-induced defects on carrier lifetime and mobility in Sn–Pb mixed perovskites. These findings suggest that Sn–Pb mixed perovskites hold great potential for space photovoltaic applications due to their superior stability under severe space radiation environments.

Introduction

For space solar power applications, photovoltaic cells are exposed to high-energy charged particle irradiation from space, which severely degrades the cells' photovoltaic performance.[1] Compared to the commercially available III–V multijunction solar cells currently used on satellites, halide perovskite solar cells (PSCs) exhibit greater radiation tolerance,[2] along with several advantages, such as flexibility, low cost, high power conversion efficiency (PCE), and light weight, which make them highly suitable for space power systems. Moreover, environmental factors that critically affect the stability of halide perovskites on Earth, such as humidity and oxidative degradation in air, are not significant concerns in the vacuum and dry conditions of space. As a result, PSCs have been regarded as one of the most promising candidates for next-generation space photovoltaic technologies.

[a] State Key Laboratory of Solar Activity and Space Weather, National Space Science Center, Chinese Academy of Sciences, Beijing, China.
E-mail: chenrui2010@nssc.ac.cn, myq@nssc.ac.cn

[b] College of Physics and Optoelectronics, Taiyuan University of Technology, Taiyuan, China. E-mail: lishiqi@tyut.edu.cn

Giving the diversity of PSCs, determining which types of perovskites are optimal for space applications remains an open question. To date, NASA has evaluated the performance of various PSCs on the International Space Station over periods of one or two years, demonstrating their good stability in low Earth orbit (LEO) environments.[3] However, for extended missions in medium Earth orbit (MEO) or geostationary Earth orbit (GEO), where the radiation environment is significantly harsher, the long-term stability of PSCs remains uncertain. In contrast to LEO, where trapped protons from the inner Van Allen radiation belt are the primary concern, MEO and GEO environments are characterized by high-energy electrons and ultraviolet (UV) light, which are more challenging to shield against and contribute to the total ionizing dose (TID) effect, leading to perovskite degradation. To assess the TID tolerance of PSCs, ground-based ^{60}Co γ-ray irradiation tests are commonly employed as an accelerated and equivalent testing method. Several studies have reported γ-ray irradiation tests on mixed-cation perovskites with the total ionizing doses reaching tens of kGy. These results indicate that γ-rays generally cause perovskite decomposition, and the radiation tolerance of perovskites is closely related to their specific compositions.[4]

On the other hand, the selection of perovskite materials for space missions must also consider the realization of high

power conversion efficiency (PCE). As the performance of single-junction perovskite solar cells approaches its theoretical limit, practical strategies to further enhance PCE increasingly rely on tandem solar cell architectures. Among various tandem configurations, all-perovskite tandem solar cells are considered the most promising for space applications. To date, tin–lead (Sn–Pb) mixed perovskites represent the only viable material system for constructing efficient all-perovskite tandem cells due to its adjustable gap. Moreover, Sn–Pb mixed perovskites exhibit many advantages, such as, high carrier mobility, long carrier lifetime, and low exciton binding energy, *etc.* A recent report suggested that the Sn–Pb tandem cell's PCE reached 27.3%.[5] The only problem for Sn–Pb perovskites is the susceptibility of Sn^{2+} to oxidize into Sn^{4+}, which introduces P-type defects that alter the band structure and hinder the carrier transport across device layers. Whether such an instability issue of Sn–Pb perovskites persists in the space radiation environment remains unclear and requires further investigation.

In this work, to clarify the Sn–Pb mixed PSCs' tolerance to the TID effect induced by space radiation, we performed a γ-ray irradiation test on the $CH_3NH_3Pb_{0.7}Sn_{0.3}I_3$-based devices and evaluated the photovoltaic performance change due to the TID effect. For comparison, the same irradiation test was performed on reference devices based on the pure Pb perovskite $CH_3NH_3PbI_3$. The results demonstrate that, compared to pure Pb perovskites, Sn–Pb mixed perovskites exhibit superior radiation stability, suggesting their greater potential for use in space power applications.

Experimental and simulation method

(a) PSC preparation

To obtain the best photovoltaic performance, we adopted a p–i–n architecture for Sn–Pb mixed and n–i–p architecture for pure Pb PSCs, respectively (Fig. 1). All the devices are without encapsulant, but kept in a plastic sample bag with a nitrogen atmosphere. The preparation of Sn–Pb mixed and pure Pb PSCs was carried out as follows. ITO conductive glass was ultrasonically cleaned in deionized water, acetone, and isopropanol for 15 min each, dried with a high-pressure air gun, and then exposed to UV light for 15 min before use.

Preparation of Sn–Pb mixed PSCs. The cleaned ITO conductive glass was spin-coated with PEDOT:PSS at 4500 rpm as the hole transport layer, followed by annealing at 130 °C for 15 min in ambient air. A precursor solution for the two-step method was prepared by dissolving 419.5 mg PbI_2 and 145.3 mg SnI_2 in a mixed solvent of 900 μL DMF and 100 μL DMSO. The solution was heated at 90 °C for 2 h and filtered through a PTFE syringe filter. A separate cation solution was prepared by dissolving 60 mg FAI, 6 mg MABr, and 6 mg MACl in 1 mL isopropanol. The anion solution was spin-coated onto the PEDOT:PSS-coated ITO substrate at 1950 rpm for 35 s. The film was then left undisturbed in a glovebox for 20 min. Subsequently, the cation solution was statically spin-coated at 1600 rpm for 30 s. Immediately after spin-coating, the film was annealed at 50 °C for 90 s, followed by a second annealing step at 120 °C for 10 min (all annealing steps
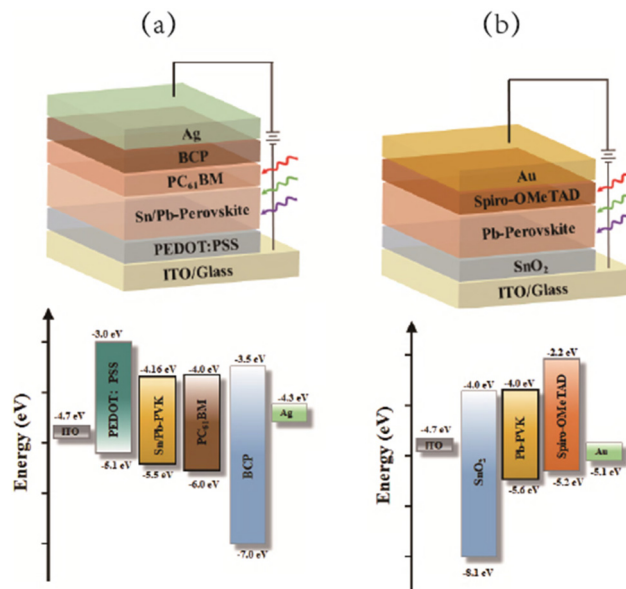

Fig. 1 Schematic views of the multiple layered architecture of the (a) Sn–Pb mixed PSC and (b) pure Pb PSC used in this work. The corresponding energy structure is shown below.

were performed in the glovebox). Finally, a $PC_{61}BM$ layer (20 mg mL^{-1} in chlorobenzene) was spin-coated at 3000 rpm as the electron transport layer, a BCP layer (0.5 mg mL^{-1} in isopropanol) was then spin-coated at 5500 rpm as the hole-blocking layer and a 100 nm-thick Ag cathode was deposited *via* thermal evaporation under vacuum.

Preparation of pure Pb PSCs. A SnO_2 thin film was spin-coated onto the pre-cleaned ITO substrate at 4000 rpm as the ETL, using a commercially purchased SnO_2 aqueous colloidal dispersion diluted 5-fold with deionized water. After spin-coating, the SnO_2 film was annealed on a hotplate at 180 °C for 20 min, followed by UV irradiation for 15 min. 599.3 mg of PbI_2 was dissolved in a mixed solvent of 900 μL DMF and 100 μL DMSO (anion solution). 60 mg of FAI, 6 mg of MABr, and 6 mg of MACl were dissolved in 1 mL of isopropanol (cation solution). The PbI_2 solution was spin-coated onto the SnO_2-coated ITO substrate at 1500 rpm for 30 s, followed by annealing at 70 °C for 1 min. After cooling to room temperature, the cation solution was spin-coated at 1700 rpm for 30 s, and the resulting film was annealed at 120 °C for 30 min to form the perovskite layer. 72.3 mg of spiro-OMeTAD, 28 μL of TBP, and 17.5 μL of Li-TFSI solution (520 mg mL^{-1} in acetonitrile) were mixed in 1 mL of chlorobenzene, stirred for 1 h, and filtered before use. The spiro-OMeTAD solution was dynamically spin-coated onto the perovskite film at 3000 rpm (20 μL volume, 30 s). The coated film was then transferred to a dry cabinet (5–10% humidity) for 24 h of oxidation. Finally, an 80 nm-thick Au anode was deposited *via* thermal evaporation.

(b) γ-Ray irradiation test

The γ-ray irradiation was performed using a ^{60}Co irradiation source. Both perovskite films and encapsulated PSCs of Sn–Pb mixed ($CH_3NH_3Pb_{0.7}Sn_{0.3}I_3$) and pure Pb-based ($CH_3NH_3PbI_3$) perovskites were prepared for the test. All samples were

Table 1 Irradiation dose conditions for pure Pb and Sn–Pb mixed PSCs

Samples	Perovskites	Irradiation dose
Perovskite film	Pure Pb	0, 0.75, 10, 30 kGy
	Sn–Pb	0, 0.75, 10, 30 kGy
Encapsulated PSCs	Pure Pb	0, 0.75, 10
	Sn–Pb	0, 0.75, 10

exposed to irradiation directly without any shielding. Since the γ-ray easily passes through the entire device with negligible energy loss, the incident direction (from n-to-p or from p-to-n) does not bring significant radiation tolerance difference.

The samples were divided into three groups, with the total ionizing doses (TID) being 0.75 kGy, 10 kGy, and 30 kGy, respectively (Table 1). The 30 kGy TID corresponds to a MEO or GEO mission for about 30 years. Each group contained three identical samples to minimize the impact of measurement variability during photovoltaic characterization. For the encapsulated solar cells, current–voltage (J–V) characteristics and PCEs were measured before and after irradiation. For the perovskite films, scanning electron microscopy (SEM) and X-ray diffraction (XRD) analyses were conducted to investigate microstructural degradation induced by radiation. Photovoltaic performance measurements of the irradiated samples were completed within 72 hours post-irradiation, with the samples stored under vacuum ($\sim 10^{-3}$ Pa) at room temperature during this period to prevent environmental degradation.

(c) Monte-Carlo simulations

To elucidate the microscopic decomposition mechanism of PSCs, we applied the Monte Carlo simulations of H^+ projecting onto the PSC devices using the transport of ions in matter (TRIM) code. Although the radiation effects on PSCs are different (TID effect for γ-rays, while displacement damage dose effect for H^+), the radiation induced damage is directly related to the formation and properties of the defects, which can be statistically analysed using the TRIM code. Here, we carried out the TRIM simulations to compare the defect types and concentrations between Sn–Pb and pure Pb PSCs under the same irradiation, rather than explicitly simulating the irradiation experiments. We comparatively simulated the 1 MeV H^+ incidence onto both the pure Pb and Sn–Pb mixed PSCs. The simulation results for the distribution of the total vacancy are created due to the collision events between incident protons (energy of 1 MeV and fluence of 10^5 H^+ per cm^2) and host atoms in the layers that constitute the solar cell architecture. In the simulations, for the target atoms (Sn, Pb) as well as for iodine, a displacement energy of 25 eV was considered to estimate the damage. The displacement energy is the minimum energy needed to displace an atom to create a vacancy. For the lighter elements like H the displacement energy was 10 eV, whereas a displacement energy of 28 eV was used for C.

Results and discussion

(a) TID effect on PSCs

Fig. 2 presents the J–V curves of the (a) Sn–Pb mixed and (b) pure Pb PSCs with exposure to various γ-ray irradiation doses.

The corresponding PCEs of the (a) Sn–Pb mixed and (b) pure Pb PSCs with exposure to various γ-ray irradiation doses are given in (c) and (d), which contain 20 sets of devices for each dose point. The average values of the photovoltaic parameters of Sn–Pb mixed and pure Pb PSCs with exposure to various γ-ray irradiation doses are further summarized in Table 2. Control devices of Sn–Pb mixed PSCs without irradiation exhibit the typical average PCE of 15.652%, with a short-circuit current density (J_{SC}) of 27.086 mA cm^{-2}, an open-circuit voltage (V_{OC}) of 0.766 V, and a fill factor (FF) of 75.455%, which is comparable with results of planar perovskite solar cells in the literature.[6] As a comparison, control devices of pure Pb PSCs without irradiation exhibit the average PCE of 20.200%, with J_{SC} 22.717 mA cm^{-2}, V_{OC} 1.156 V, and FF 76.938. After the γ-ray irradiation with TID of 0.75 kGy, the PCE of Sn–Pb mixed PSCs has decreased by 31%, whereas that of pure Pb PSCs degrades more severely, with a reduction of 48%. It is evident that the Sn–Pb mixed PSCs exhibit significantly better TID tolerance than the pure Pb PSCs. By analyzing the degradation of V_{OC}, J_{SC}, and FF, we find that a substantial contributor to PCE loss is the decrease in FF. Since FF is closely related to carrier recombination mechanisms—where a higher FF typically indicates dominance of radiative recombination and a lower FF suggests increased nonradiative recombination due to deep-level defects, the greater FF degradation observed in pure Pb PSCs implies a larger number of deep-level defects formed in these devices compared to Sn–Pb PSCs. According to the Shockley–Read–Hall (SRH) recombination theory, the deep-level defects act as the nonradiative centers to reduce the carrier concentration and their mobility, leading to a rapid decline in FF. This explains the pronounced FF degradation in irradiated pure Pb PSCs.

We summarize the relative decrease of the photovoltaic parameters before and after irradiation in Table 3. When the TID reaches 10 kGy, the PCE of the Sn–Pb mixed PSCs is decreased by 67%, whereas pure Pb PSCs suffer a much greater loss of 90% in PCE. The FF decreases by 31% for Sn–Pb mixed
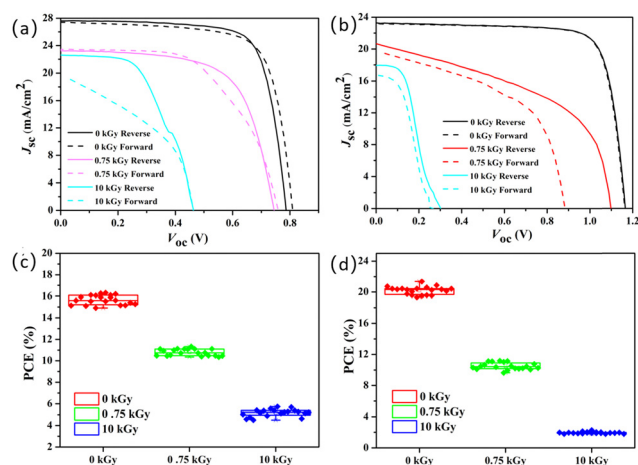
Fig. 2 J–V curves of the (a) Sn–Pb mixed and (b) Pb PSCs before and after ^{60}Co γ-ray irradiation with varying TID conditions, and the corresponding PCE after various-dose irradiations for (c) Sn–Pb mixed and (d) Pb PSCs.

Table 2 Photovoltaic parameters of Sn–Pb mixed (in bold) and pure Pb PSCs (in italics) after γ-ray irradiation with varying TID conditions

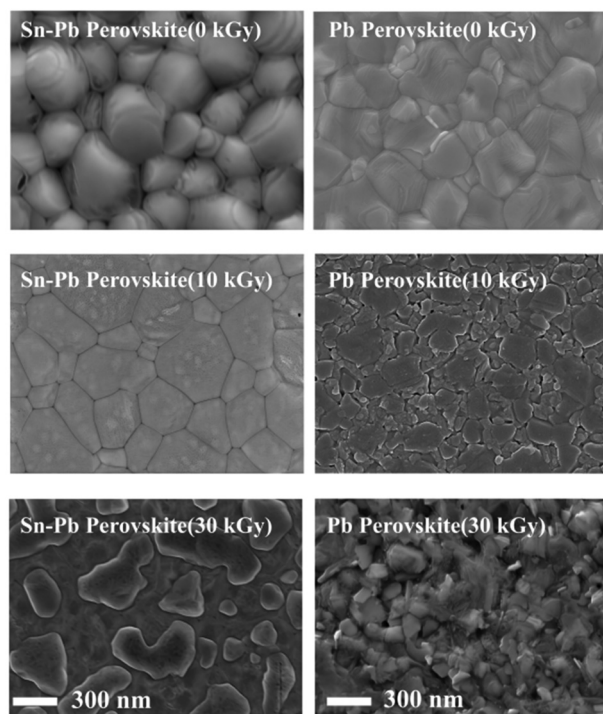| TID	V_{OC} (V)	J_{SC} (mA cm^{-2})	FF (%)	PCE (%)
0 kGy	**0.766**	**27.086**	**75.455**	**15.652**
	1.156	*22.717*	*76.938*	*20.200*
0.75 kGy	**0.734**	**22.775**	**64.514**	**10.783**
	1.085	*19.867*	*48.632*	*10.485*
10 kGy	**0.455**	**21.667**	**52.330**	**5.166**
	0.288	*16.605*	*40.643*	*1.947*

PSCs, compared to a 47% reduction in pure Pb PSCs. The relative decrease in J_{SC} is 20% for Sn–Pb mixed PSCs and 24% for pure Pb PCSs after 10 kGy irradiation. Notably, the relative decrease of V_{OC} is more severe for pure Pb PSCs (75%) compared to Sn–Pb mixed PSCs (40%). Since V_{OC} is closely related to the bandgap of the perovskite material, its reduction serves as a clear indicator of structural or crystalline degradation under high-dose irradiation, which will be further discussed in the following section.

(b) TID effect on perovskite films

Since the PSCs are composed of multiple functional layers, it is important to determine whether the degradation of the perovskite layer is the dominant factor contributing to the overall decline in photovoltaic performance. To address this, Fig. 3 demonstrates the top-view scanning electron microscope (SEM) images of both the Sn–Pb mixed and pure Pb perovskite films before and after γ-ray irradiation. As shown, when the TID reaches 10 kGy, the Sn–Pb mixed perovskite film largely retains its crystalline structure, with grain sizes around 300 nm. In contrast, the pure Pb perovskite film exhibits severe decomposition, with numerous grain boundaries being formed, which likely hinders carrier transport through the film. The disruption of the crystalline grains is closely associated with radiation-induced defect formation dynamics. As previously discussed, a higher density of defects is formed in the pure Pb perovskite than in the Sn–Pb mixed perovskite. These defects migrate and accumulate, ultimately causing local crystalline structural degradation of the pure Pb perovskite. We further examined samples exposed to a TID of up to 30 kGy. Under these conditions, the crystalline structure of the pure Pb perovskite film has been completely destroyed. In contrast, the Sn–Pb mixed perovskite still maintains visible crystalline grains, although a phase-separation-like behavior becomes apparent. We notice that such a phase separation in Sn–Pb mixed perovskite under irradiation in ambient air was also reported elsewhere in ref. 7. That study suggested that Pb-rich regions appear on the surface after Sn^{2+}

Fig. 3 SEM image of the Sn–Pb mixed and Pb perovskite film after γ-ray irradiation with a total ionization dose of 0, 10 and 30 kGy, respectively.

oxidation, and these Pb-rich regions are reconstituted from the yellow phase of formamidinium lead iodide to the black phase with prolonged irradiation. In our case, however, Sn–Pb mixed perovskite films were stored under vacuum before and after γ-ray irradiation, minimizing any oxygen-related reactions. Despite this controlled environment, the phase separation phenomenon is still observed, indicating that the high-dose TID effect alone can induce such structural changes. This irreversible phase reconstruction appears to be a common stage in the degradation pathway of Sn–Pb perovskites under radiation, regardless of atmospheric conditions.

To further investigate the crystalline phase changes induced by the TID effect, we conducted the X-ray diffraction (XRD) measurement of the Sn–Pb mixed and pure Pb PSC films (a) before and after γ-ray irradiation with the TID 30 kGy, as shown in Fig. 4. Evidently, due to the TID effect, the crystalline structure is destroyed for both Sn–Pb and pure Pb perovskite films, which is reflected by the broadening of the diffraction peak (peak $2\theta = 13.9°$ corresponds to the orientation of (110)). The point is that the broadening of the diffraction peak of the pure Pb film is more severe than that of the Sn–Pb mixed film. Moreover, we can see that many additional diffraction peaks emerge for both Sn–Pb mixed and pure Pb films due to irradiation, indicating the destruction of the ABX$_3$-type perovskite structure. One special additional peak is $2\theta = 12.8°$, which is the typical indicator for the appearance of PbI$_2$, and only appears for pure Pb film but not for the Sn–Pb mixed film. This is also evidence that the pure Pb perovskite film is easier to decompose than the Sn–Pb perovskite film. The XRD measurements are consistent with the SEM results, where the complete
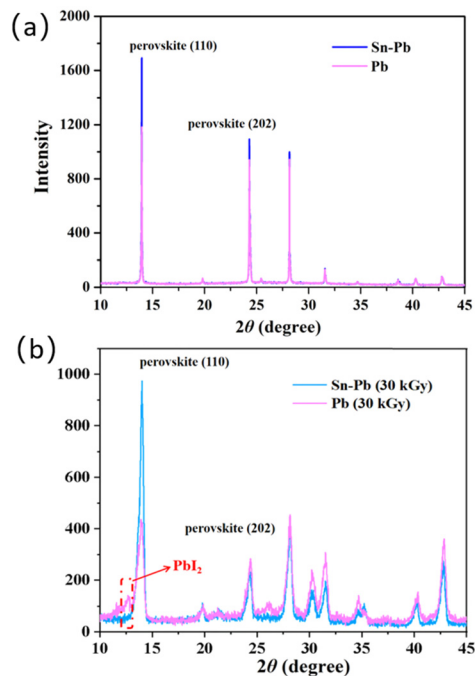
Table 3 Relative decrease (RD) of photovoltaic parameters of Sn–Pb mixed (in bold) and pure Pb (in italics) before and after γ-ray irradiation

TID	RD of V_{OC} (%)	RD of J_{SC} (%)	RD of FF (%)	RD of PCE (%)
0.75 kGy	**4**	**16**	**15**	**31**
	6	*13*	*37*	*48*
10 kGy	**40**	**20**	**31**	**67**
	75	*27*	*47*	*90*

Fig. 4 XRD spectra of the Sn−Pb and Pb halide perovskite film (a) before and (b) after the 30 kGy γ-ray radiation.

decomposition of perovskite was shown for the pure Pb perovskite film, but it is less severe for the Sn–Pb mixed perovskite film.

(c) The degradation of the HTL and ETL

Noting that the Sn–Pb mixed and pure Pb PSCs exhibit a different hole transport layer (HTL) and electron transport layer (ETL), we need to further clarify whether the radiation tolerance also stems from the device structure variations. In ref. 8, such a topic has been discussed in detail. Two of their PSC devices have the same pure Pb perovskite layer but with different charge transport layers, which are similar to those in our work. We notice that after an electron irradiation dose up to 100 kGy, the PCE decline for these two devices is not significantly different (45% for the p–i–n device and 56% for the n–i–p device, see Table 4). This indicates that the TID effect on the different charge transport layers does not introduce significant variation for the device's radiation tolerance. Considering that the Sn–Pb mixed perovskite film exhibits significantly better radiation tolerance than the pure Pb perovskite film, we can conclude that the different PCE decline for the Sn–Pb mixed and pure Pb perovskite device are primarily attributed to the radiation tolerance variation of the perovskite layers.

(d) TRIM simulation results

Fig. 5 presents a comparative analysis of the TRIM simulation results for 1 MeV H$^+$ incident on Sn–Pb mixed and pure Pb PSCs. Fig. 5(a1) and (b1) illustrate the ion track of the 1 MeV protons passing through the device layers of the Sn–Pb mixed and pure Pb PSCs, respectively. These results indicate that 1 MeV H$^+$ could fully penetrate the entire device structure.

Table 4 Architectures of two devices in ref. 8 and the relative decline of PCE due to electron irradiation up to 100 kGy

Device/ architecture	HTM	ETM	PCE (%)	RD of PCE (%)
1 p–i–n	Spiro-OMeTAD	c-TiO$_2$/mpTiO$_2$	Before: 18.2 After: 10.1	45
2 n–i–p	PEDOT:PSS	PCBM/PDINO	Before: 9.9 After: 4.3	56

Fig. 5(a2) and (b2) demonstrates the individual contributions of the vacancies associated with the constituent elements in the layers of PSCs. We can identify that iodine-related vacancies account for the largest proportion ($\sim 50\%$) to the total vacancies, whereas Sn and Pb contribute less than 10% of the total vacancies. The H atoms present in the layer contribute to slightly above 10% of the total vacancies. According to the principles of mass and charge conservation, the generation of vacancies is accompanied by the formation of other defect types, such as interstitials and antisites. Although these are not directly shown in Fig. 5, they are expected to occur in comparable quantities and may significantly influence the photovoltaic performance of irradiated PSCs. As shown in Fig. 5(a2) and (b2), the number of iodine recoils in Sn–Pb mixed perovskite is approximately 20% lower than that in pure Pb perovskite. This indicates that both the iodine interstitial (I_{int}) and iodine vacancy (V_I) are less prevalent in Sn–Pb mixed perovskite compared to their pure Pb counterparts. A detailed first-principles study on the defects and properties of Sn–Pb mixed perovskite was previously reported in ref. 9. That work revealed that Sn–Pb mixed perovskite films exhibit stronger B–X ionic bonding strength, which could diminish the replacement of iodine and enhance the resilience of the local damage to recover
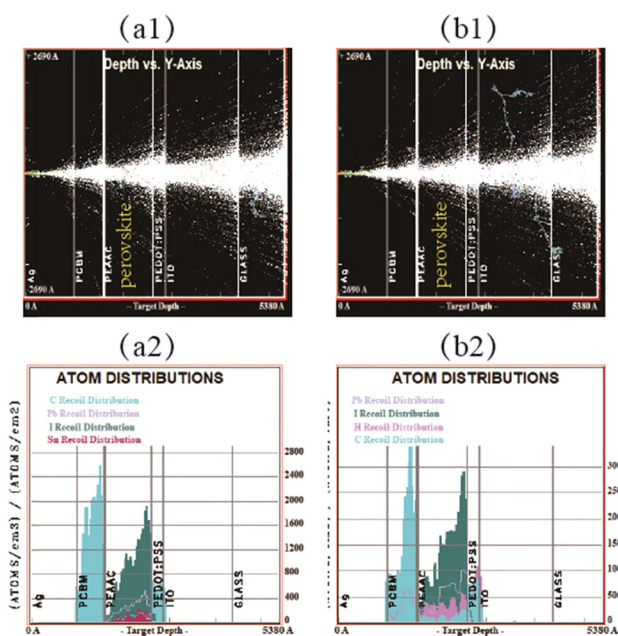

Fig. 5 Ion tracking of 1 MeV H$^+$ projecting into the (a1) Sn–Pb and (b1) pure Pb PSCs, and the corresponding atomic recoil distributions, (a2) and (b2).
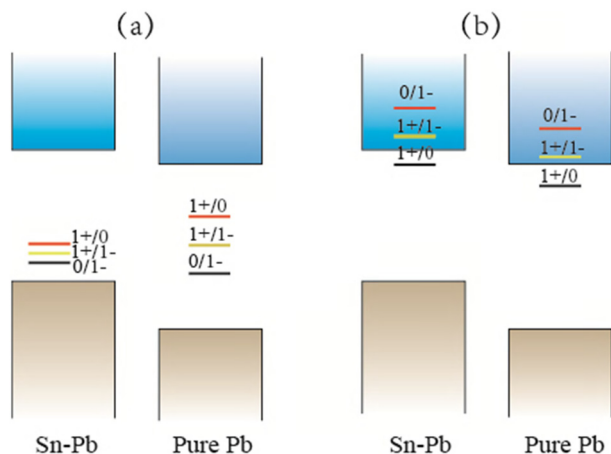
Fig. 6 Charge transition levels of defects (a) I_{int} and (b) V_I for Sn–Pb and pure Pb perovskites.[8] The symbols 0, 1+, and 1− represent the charge state of the defect.

the crystalline phase. Based on these findings, we conclude that the reduced concentration of iodine-related defects in Sn–Pb mixed perovskites compared to pure Pb perovskite is the primary factor contributing to their superior tolerance to TID effects.

The key factor to cause the crystal structure destruction is the displacement of the halide atom, which has been a famous issue for the perovskite solar cell's stability problem. In ref. 10, it has been reported that the ion migration in Sn–Pb mixed perovskite can be significantly suppressed. By employing scan-rate-dependent current–voltage measurements on Pb and mixed Pb–Sn perovskite solar cells, they evaluated the short circuit current losses at lower scan rates and traced the presence of the mobile ions. It was found that the iodine ions in Sn–Pb mixed perovskite are harder to migrate than that in pure Pb perovskite. Meanwhile, the first-principles calculations also revealed that the existence of Sn vacancies plays an important role for suppressing the iodine migration by forming an energy barrier across the iodine migration trace. This explains why Sn–Pb perovskites exhibit better radiation tolerance than pure Pb perovskite. Radiation creates iodine-related defects as well as the Sn and Pb vacancies; however, the existence of Sn vacancies suppressed the iodine migration, which hinders the further decomposition of the crystal structure.

Except for comparing the radiation generated iodine-related defect concentrations, we also compared the characteristic of a single iodine defect between Sn–Pb mixed and pure Pb perovskite. Referring to the first principles calculation results in ref. 9, we show a schematic view of the charge transition levels (CTLs) of defects I_{int} and V_I in Fig. 6, for both the pure Pb and Sn–Pb mixed perovskite films. The physical meaning of CTL can be regarded as the Fermi level at which the corresponding charged defects are formed. Therefore, we can judge that such charged defects are deep level state or shallow level state by observing the relative locations of the CTLs to the CBM (conduction band minimum) and VBM (valence band maximum). As shown in Fig. 6, one can identify that the CTLs of V_I locate near the CBM for both pure Pb and Sn–Pb mixed perovskite,

indicating that V_I are shallow defects for both perovskites. On the contrary, CTLs of I_{int} behave as deep levels within the gap of pure Pb perovskite, but locate near the VBM for the Sn–Pb perovskite. Such a difference of I_{int} CTL can be attributed to the VBM of Sn–Pb being much higher than that of pure Pb perovskite. Then it is clear that I_{int} are deep defects in pure Pb perovskite but shallow defects in Sn–Pb mixed perovskite. Deep defects act as the nonradiative recombination centers for charge carriers and thus decrease the carrier lifetime and mobility, while shallow defects act as carrier trapping and detrapping centers, which has less impact on the carriers' lifetime and mobility. The different carrier–I_{int} interaction characteristics between Sn–Pb and pure Pb perovskite explain why the relative decrease of J_{SC} for pure Pb (24%) is larger than that of Sn–Pb (20%).

Summarizing the above discussions, we finally reach the conclusions of why Sn–Pb mixed PSCs exhibit more radiation resistance than pure Pb PSCs: (1) radiation generates less iodine defects in Sn–Pb mixed perovskite film compared to pure Pb perovskite film, which further makes the Sn–Pb crystalline phase harder to degrade by radiation; (2) iodine interstitials are a shallow-level defect in Sn–Pb but a deep-level defect in pure Pb perovskite, which determines that the carriers' lifetime and mobility are less affected by radiation in the Sn–Pb perovskite. Therefore, Sn–Pb mixed PSCs exhibit superior radiation tolerance compared to pure Pb PSCs.

Conclusions

To conclude, we compared the TID effect tolerance of Sn–Pb and pure Pb PSCs by applying the ^{60}Co γ-ray irradiation experiment. We found that Sn–Pb mixed PSCs demonstrate superior TID resistance to the TID effect than pure Pb PSCs. By applying photovoltaic measurements and Monte Carlo simulations, we find that the better TID tolerance of Sn–Pb mixed PSCs can be attributed to the relatively low iodine defect concentrations under the TID effect. The low-concentration of iodine defects further means that the broken crystalline phase is less significant in Sn–Pb perovskite, which was proven by the XRD spectrum and the SEM image of the irradiated Sn–Pb perovskite film with TID up to 30 kGy. Our study suggests that Sn–Pb perovskite could be a better choice for space power applications, especially for those long-period missions with a high cumulative TID. This also further suggests that the Sn–Pb based all-perovskite tandem solar cell might be a promising solution for space power by simultaneously satisfying the high PCE requirement and the stability requirement in the space radiation environments.

Author contributions

Longlong Zhang contributed to the conception of this study, performed the data analyses and wrote the manuscript; Shiqi Li contributed to the preparation of the samples and the photovoltaic measurement; Yinghao Wang contributed to the SEM

measurement; Hongwei Li, Xiang Zhu, and Xiaoheng Xu helped with the data analysis and plotting; Yuying Hao helped with the discussions; Yingqi Ma and Rui Chen helped with funding acquisition.

Conflicts of interest

No conflict of interest exists in the submission of this manuscript.

Data availability

The raw data of this work are available at DOI: **https://doi.org/10.57760/sciencedb.space.02885**.

Acknowledgements

References

1 R. Y. Loo, G. S. Kamath and S. S. Li, *IEEE Trans. Electron Devices*, 1990, **37**(2), 485; M. V. Ryabtseva, A. S. Petrov and G. S. Voevodkin, *et al.*, *Microelectron. Reliab.*, 2021, **125**, 114305; J. Li, A. Aierken and Y. Zhuang, *et al.*, *Sol. Energy Mater. Sol. Cells*, 2021, **224**, 111022.

2 Y. Miyazawa, M. Ikegami and H.-W. Chen, *iScience*, 2018, **2**, 148; O. Malinkiewicz, M. Imaizumi, S. B. Sapkota, T. Ohshima and S. Öz, *Emerging Mater. Res.*, 2020, **3**, 9–14; F. Lang, M. Jost and K. Frohna, *et al.*, *Joule*, 2020, **4**, 1054; A. R. Kimani, T. A. Byers and Z. Ni, *et al.*, *Nat. Commun.*, 2024, **15**, 696; Z. Song, C. Li and C. Chen, *et al.*, *J. Phys. Chem. C*, 2019, **124**, 1330.

3 W. Delmas, S. Erickson and J. Arteaga, *et al.*, *Adv. Energy Mater.*, 2023, **13**, 2203920; T. S. Krause and K. T. Vansant, *et al.*, *RRL Solar*, 2023, **7**, 2300468.

4 L. Gao, K. Tao, J. L. Sun and Q. Yan, *Adv. Opt. Mater.*, 2022, **10**, 2102069; A. G. Boldyreva, A. F. Akbulatov, S. A. Tsarev, S. Y. Luchkin, I. S. Zhidkov and E. Z. Kurmaev, *J. Chem. Phys. Lett.*, 2019, **10**, 813; S. Yang, Z. Xu and S. Xue, *et al.*, *Adv. Mater.*, 2019, **31**, 1805547; K. Huang, K. Yang and H. Li, *ACS Appl. Energy Mater.*, 2020, **3**, 7318; Z. Huan, Y. Zheng and K. Wang, *et al.*, *J. Mater. Chem. A*, 2024, **12**, 1910.

5 D. Yu, M. Pan, G. Liu, X. Jiang, X. Wen and W. Li, *et al.*, *Nat. Energy*, 2024, **9**, 298.

6 X. Xue, L. Zhang and Y. Hao, *et al.*, *ACS Mater. Lett.*, 2023, **5**, 1601; H. Lee, S. B. Kang and S. Lee, *Nano Convergence*, 2023, **10**(27), 9448; F. Zuo, S. T. Williams and P. W. Liang, *et al.*, *Adv. Mater.*, 2014, **26**, 6454.

7 W. Li, Z. Li, S. Zhou, Y. Gou, G. Li and J. Li, *et al.*, *Nat. Commun.*, 2025, **16**, 506.

8 Y. Murakami, R. Nishikubo, F. Ishiwari, K. Okamoto, T. Kozawa and A. Saeki, *et al.*, *Mater. Adv.*, 2022, **3**, 4861.

9 J. Xu, A. Maxwell, M. Wei, Z. Wang, B. Chen and T. Zhu, *et al.*, *ACS Energy Lett.*, 2021, **6**, 4220.

10 K. Dey, D. Ghosh, M. Pilot, S. R. Pering, B. Roose and P. Deswal, *et al.*, *Energy Environ. Sci.*, 2024, **17**, 760.